


# A microstructure model for viscoelastic-thixotropic fluids

Cite as: Phys. Fluids **32**, 123106 (2020); <https://doi.org/10.1063/5.0033199>

Submitted: 15 October 2020 . Accepted: 04 December 2020 . Published Online: 29 December 2020

 K. Le-Cao,  N. Phan-Thien,  N. Mai-Duy,  S. K. Ooi,  A. C. Lee, and  B. C. Khoo

## COLLECTIONS

 This paper was selected as Featured



View Online



Export Citation



CrossMark

## ARTICLES YOU MAY BE INTERESTED IN

[A comparative study of quasi-stable sheet cavities at different stages based on fast synchrotron x-ray imaging](#)

Physics of Fluids **32**, 123316 (2020); <https://doi.org/10.1063/5.0031433>

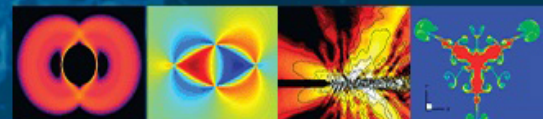
[Turbulent flow and heat flux analysis from validated large eddy simulations of flow past a heated cylinder in the near wake region](#)

Physics of Fluids **32**, 125119 (2020); <https://doi.org/10.1063/5.0031831>

[The perspective of fluid flow behavior of respiratory droplets and aerosols through the facemasks in context of SARS-CoV-2](#)

Physics of Fluids **32**, 111301 (2020); <https://doi.org/10.1063/5.0029767>

Physics of Fluids  
**GALLERY OF COVERS**



# A microstructure model for viscoelastic–thixotropic fluids

Cite as: *Phys. Fluids* **32**, 123106 (2020); doi: [10.1063/5.0033199](https://doi.org/10.1063/5.0033199)

Submitted: 15 October 2020 • Accepted: 4 December 2020 •

Published Online: 29 December 2020



View Online



Export Citation



CrossMark

K. Le-Cao,<sup>1</sup>  N. Phan-Thien,<sup>1,a)</sup>  N. Mai-Duy,<sup>2</sup>  S. K. Ooi,<sup>3</sup>  A. C. Lee,<sup>3</sup>  and B. C. Khoo<sup>1</sup> 

## AFFILIATIONS

<sup>1</sup>Department of Mechanical Engineering, National University of Singapore, 9 Engineering Drive 1, Block EA 07-08, Singapore 117575

<sup>2</sup>School of Mechanical and Electrical Engineering, University of Southern Queensland, 487-535 West Street, Toowoomba, QLD 4350, Australia

<sup>3</sup>Tropical Marine Science Institute, National University of Singapore S2S, 18 Kent Ridge Road, Singapore 119227

<sup>a)</sup>Author to whom correspondence should be addressed: [nhan@nus.edu.sg](mailto:nhan@nus.edu.sg)

## ABSTRACT

A microstructure model to describe the viscoelasticity and thixotropy properties of complex fluids is proposed. The model is based on the Lodge–Yamamoto network theory and is an extension of the Phan–Thien–Tanner model, with a kinetic process in which specific forms of creation and destruction rates are assumed. The final equation is simple with a small number of empirical parameters required and can be conveniently employed in engineering simulations. The predictions based on the model in a variety of shear and oscillatory shear flows are given. The stress response obtained from the model prediction agrees well with experiments on both shear and oscillatory flow histories.

Published under license by AIP Publishing. <https://doi.org/10.1063/5.0033199>

## I. INTRODUCTION

Thixotropy is a general term describing the time-dependent (and/or flow process dependent) response of the material. A wide range of complex fluids exhibits thixotropic behavior, including seabed sediment, coral mucus, concrete mixtures, paints, food, and some biological and pharmaceuticals products. These complex mixtures at quiescent state consist of attractive particles or chains, which constitute clusters forming a structured network of sufficient link—this network can resist any applied stress less than a certain level (in some stress measures) with an elastic response. Conversely, if the applied stress range is sufficiently large (again, in some stress measures), the structured network disintegrates and consequently results in reduced resistance to deform and flow.<sup>1,2</sup> The reverse may also occur, i.e., the mixture may recover some of its network link,<sup>3</sup> and the critical stress value of the restored state may be similar or smaller than that of the original state. The microstructure network requires time to build up and to break off, and the rheology of the fluid thus has a time scale. The forming and destruction of the microstructure network resulting in thixotropy have been simulated in Ref. 4 in a dissipative particle dynamics (DPD) framework.

To model microstructure mixtures known to be thixotropic, approaches based on a structural kinetics theory have been proposed and applied widely. The current published works can be classified into direct and indirect approaches. In these works, the degree of microstructure formation is represented by a scalar quantity  $f$ . When  $f = f_0$  (usually,  $f_0 = 1$ ), the initial structure is said to be fully developed. On the other hand,  $f = 0$  implies an entirely collapsed network when a steady state is achieved. A detailed review can be found in, e.g., Refs. 5–8. In the direct micro-structural approach,  $f$  can be directly linked to the description of the dynamics of the microstructure network (e.g., a number of network bonds found at that time).<sup>6</sup> Typical studies include the works of Goodeve,<sup>3</sup> Storey and Merrill,<sup>9</sup> Liu *et al.*,<sup>10</sup> De Kee and Chan,<sup>11,12</sup> and Soong and Shen.<sup>13</sup> In contrast, in the indirect microstructure approach,<sup>6</sup>  $f$  is simply a particular microstructure degree description characterized by a scalar value, for instance, in the works of Moore,<sup>14</sup> Cheng and Evans,<sup>15</sup> Tiu and Boger,<sup>16</sup> Dimitriou and McKinley,<sup>17</sup> and de Souza Mendes.<sup>18</sup>

Both types of theories are similar in introducing the thixotropy via a total time derivative of the structured parameter  $f$  in a first-order rate kinetic process,

$$\frac{df}{dt} = \frac{\partial f}{\partial t} + u_x \frac{\partial f}{\partial x} = K_1(f) - K_2(f, \dot{\gamma}), \quad (1)$$

where  $u_x$  is the only  $x$ -component of the velocity vector (one-dimensionality is assumed here for simplicity);  $K_1(f)$  and  $K_2(f, \dot{\gamma})$  are the two (possibly shear-rate dependent) functions for the rate of build-up and breakdown of the microstructure, respectively.

## II. REVIEW OF MICROSTRUCTURAL MODELS

### A. Simple thixotropy models

In the simple thixotropy models, the structure evolution [Eq. (1)] is linked with the mixture viscosity (the most important piece of information in engineering calculations), which may be shear thinning (or thickening), and a yield stress could be introduced. For example, Toorman<sup>19</sup> proposed a model based on Moore's.<sup>14</sup> The Toorman model has five parameters, four of which can be found from the fluid equilibrium state. The last one can be determined by a transient experiment. The model is a useful and practical mathematical model of cohesive sediments. Another well-known one is Coussot *et al.*'s model.<sup>20</sup> The authors linked the fluid microstructure of a clay suspension to its behavior in a gravity-driven flow and pointed out that the microstructure evolution has a strong effect on the flow dynamics.<sup>21</sup> In Ref. 22, a fitting procedure was proposed to determine the model parameters. The model has been shown to successfully predict the flow characteristics. Bekkour *et al.*<sup>23</sup> investigated the dependence of a bentonite clay microstructure build-up/breakdown rate on the clay. For food products, such as a mayonnaise mixture, a phenomenological model of Tiu and Boger<sup>16</sup> has been used and satisfactory results were obtained.

We briefly review the simple "viscous-thixotropy fluid" model for completeness; here, one has  $f$  evolving in time according to Eq. (1) with  $K_1(f) = a(f_0 - f)$  and  $K_2(f, \dot{\gamma}) = b\dot{\gamma}f$ ,

$$\frac{d}{dt}f = a(1 - f) - b\dot{\gamma}f = a - (a + b\dot{\gamma})f, \quad (2)$$

where  $a$  is the rate of creation of the structure and the rate of destruction of the structure is proportional to the magnitude shear rate  $\dot{\gamma}$ , with a proportional constant  $b$ . This may be rewritten as

$$\frac{d}{dt}f = \lambda_0^{-1} - \lambda_0^{-1}h(\dot{\gamma})f, \quad f(0) = f_0, \quad (3)$$

where  $\lambda_0 = a^{-1}$  is a time constant,  $h(\dot{\gamma}) = 1 + \beta\dot{\gamma}$ , and  $\beta = b/a$ . Of course,  $h$  need not be a linear function but can be any positive function of the shear rate. At equilibrium, the structured parameter is

$$f_e = \frac{1}{1 + \beta\dot{\gamma}} = \frac{1}{h(\dot{\gamma})}. \quad (4)$$

The coupling to the stress is provided via the constitutive assumption that the fluid is a generalized Newtonian fluid, with a viscosity given by

$$\eta(f) = \eta_\infty + \eta_\infty \alpha f, \quad (5)$$

where  $\alpha$  is a constitutive constant. Once the structure is entirely broken down ( $f = 0$ ), the fluid has a (low) viscosity of  $\eta_\infty$ ; when the

structure is fully built-up ( $f = 1$ ), the fluid has a (high) viscosity of  $\eta(f) = \eta_\infty(1 + \alpha)$ . The solution to (3) is

$$f = \frac{1}{h(\dot{\gamma})} \left( 1 - e^{-\lambda_0^{-1}h(\dot{\gamma})t} \right) + f_0 e^{-\lambda_0^{-1}h(\dot{\gamma})t}. \quad (6)$$

Thus, there is a relaxation time  $\lambda_0$  in an otherwise Newtonian fluid due to the built-up/breakdown of the structure.

The shear stress

$$S_{12} = \eta_\infty \alpha f \dot{\gamma} + \eta_\infty \dot{\gamma} \quad (7)$$

and its derivative

$$\frac{d}{dt}S_{12} = \lambda_0^{-1} \eta_\infty \dot{\gamma} (\alpha + h(\dot{\gamma})) - \lambda_0^{-1} h(\dot{\gamma}) S_{12} \quad (8)$$

satisfy

$$\frac{\lambda_0}{h(\dot{\gamma})} \frac{d}{dt}S_{12} + S_{12} = \frac{\eta_\infty \alpha}{h(\dot{\gamma})} \dot{\gamma}, \quad (9)$$

resembling that of a (linear) Maxwell fluid with a relaxation time of  $\lambda_0/h(\dot{\gamma})$ .

A yield stress  $S_0$  can and has been introduced to the stress equation (Refs. 19 and 24),

$$S_{12} = fS_0 + \eta_\infty(1 + \alpha f)\dot{\gamma}. \quad (10)$$

At  $f = f_e$ , when the rate of breakdown equals the rate of restoration, the equilibrium flow (EF) curve is described by evaluating Eq. (10) at the equilibrium point,

$$S_e = f_e S_0 + \eta_\infty(1 + \alpha f_e)\dot{\gamma}. \quad (11)$$

References 19 and 25 showed that thixotropic mixtures may possess a group of stress/strain rate curves named constant structure curves (CSCs). An  $i$ th CSC associates to a (constant) value of  $f_i$ , which is the intersection between the CS curve and the EF curve (Fig. 1). As the EF curve can be expressed by Eq. (11), a scheme

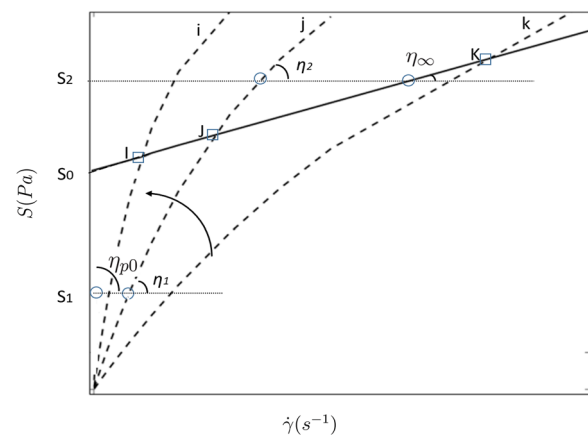


**FIG. 1.** A typical EFC (solid line) and CSCs (dash lines). I, J, K are the intersection between EFC and  $i, j, k$ th CSCs, respectively;  $\eta_{p0}$  and  $\eta_\infty$  are low and high shear viscosity of EFC; and  $\eta_1$  and  $\eta_2$  are viscosities of the  $j$ th CSC corresponding to stresses  $S_1$  and  $S_2$ . The arrow indicates that the structural levels increase.

providing the calculation of the CS curves was detailed in Ref. 19. For example, if the fitting equation for equilibrium data is the Bingham model,

$$S_{BH} = S_0 + \mu_\infty \dot{\gamma}, \quad (12)$$

then, equating (11) to Eq. (12), one has

$$\eta_\infty \dot{\gamma} = (1 - f_e)S_0 - \eta_\infty \alpha f_e \dot{\gamma} + \mu_\infty \dot{\gamma}. \quad (13)$$

Substituting Eq. (13) into Eq. (10), the rheological equation for a thixotropic (Bingham) yield stress fluid is

$$S_{12} = (1 + f - f_e)S_0 + (f - f_e)\eta_\infty \alpha \dot{\gamma} + \mu_\infty \dot{\gamma}. \quad (14)$$

Using the relation  $1 - f_e = f_e \beta \dot{\gamma}$  [Eq. (4)], Eq. (14) becomes

$$S_{12} = fS_0 + ((f - f_e)\eta_\infty \alpha + \mu_\infty + f_e \beta) \dot{\gamma}.$$

Consider a CS curve that has a unique value of the structural parameter  $f_i$ , which corresponds to an  $i$ th data point of the EF curve. The value of  $f_i$  equals to  $f_I$  at the crossover point  $I$  of this CS and the EF curves. The CS curve of the  $i$ th point can be given by substituting  $f_i$  into Eq. (14),

$$S_{12} = (1 + f_i - f_e)S_0 + (f_i - f_e)\eta_\infty \alpha \dot{\gamma} + \mu_\infty \dot{\gamma} \quad (15)$$

or

$$S_{12} = (1 + h_I^{-1} - h^{-1})S_0 + (h_I^{-1} - h^{-1})\eta_\infty \alpha \dot{\gamma} + \mu_\infty \dot{\gamma}. \quad (16)$$

The viscous–thixotropy model does quite well, especially with cohesive sediments—in particular, it shows a stress overshoot due to the long time scale of microstructures (and thus of its viscosity) in a shear flow history. In addition, the incorporation of the model into flow solvers was also reported.<sup>26–31</sup> However, thixotropy affects not only viscosity but also the whole rheology of the fluid. To illustrate this, in a sinusoidal shear flow  $\dot{\gamma} = \delta \omega \cos(\omega t)$  with the small strain amplitude  $\delta$ , one has a constant solution for (3),  $f = f_c$ . This leads to

$$\eta' = \eta_0(1 + \alpha f_c), \quad \eta'' = 0. \quad (17)$$

In order to find non-trivial  $G' = \omega \eta''$ , and  $G'' = \omega \eta'$ , some other models involving viscoelasticity need to be employed.

## B. Viscoelastic–thixotropy models

Generally, the reported viscoelastic–thixotropy models start from the microstructure evolution [Eq. (1)]; it is then coupled with a continuum viscoelastic model (e.g., Maxwell model). The approach is thus called the micro–macro approach. Similar to viscous–thixotropy models, viscoelastic–thixotropy models can be developed from both direct and indirect approaches.

Many indirect viscoelastic–thixotropy models have been reported in the literature. For example, in Ref. 32, a constitutive equation based on a network theory with the relaxation time determined by structure parameters. The model has been applied for prediction in some non-linear responses of polymer melts. Coussot *et al.*<sup>33</sup> developed a model composed of a Maxwell model and the structural kinetic equations to investigate the response of particle systems suspended in a viscoelastic medium in both steady

and transient flows. In Ref. 34, the rheological model of Coussot was further investigated and reasonably well predicted the results in structure build-up experiments. Dullaert and Mewis<sup>35</sup> introduced a general version of the structural kinetics model in which the total stress comprises of an elastic part (structure-dependent) and a viscous part. Extensions of the Dullaert and Mewis approach to large amplitude oscillatory shear (LAOS) flows have been presented by Armstrong *et al.*<sup>36</sup> A viscoelastic–thixotropy model with an elastic and a viscous part for clay suspension was presented in the work of Mujumdar *et al.*<sup>5</sup> Using a spring-like interaction between clay particles, Hermidas *et al.*<sup>37</sup> were able to decrease the amount of experimental parameters needed by the model of Mujumdar *et al.*<sup>5</sup> from 7 to 4. Yziquel *et al.*<sup>38</sup> introduced a model derived from a Jeffreys model and a kinetic equation (three types of kinetic equations were investigated) to model the microstructure evolution for concentrated colloidal suspensions. Recently, Ramya *et al.*<sup>39</sup> combined a simple yield stress thixotropic model with the Giesekus model, which is structure dependent to predict the responses of fumed silica–polyisobutylene/paraffin oil mixtures to various test flows.

For direct models, Goodeve<sup>3</sup> provided a general theoretical approach combining thixotropy and viscosity. The theory showed that the non-Newtonian viscosity usually has two distinct parts, one is Newtonian and the other is the thixotropy which can be thought of the interactions between particles and the establishment of “bonds.” The broken and reformed bonds were explained by shear and thermal mechanisms. Later, Storey and Merrill<sup>9</sup> modified the theory of Goodeve<sup>3</sup> to study two molecular species of starch solutions. In Ref. 40, Cross developed a kinetic model in which the structural formation is a result of Brownian movement and the disruption rate is an even function of strain rate. Doremus and Piau<sup>41</sup> presented a double network model based on the Yamamoto model<sup>42–44</sup> for a complex material composed of a polymer and a filler. Soong and Shen,<sup>13</sup> using a deterministic expression of the network theory and neglecting the elastic property, considered a polymer network as a set of random chains with  $n$  average number of entanglements. The loss (break-up) rate was assumed to be caused by the shear rate, and the gain (reformation) rate was allowed to depend on the thermal diffusivity. Later, Liu *et al.*<sup>10</sup> coupled the Soong and Shen<sup>13</sup> model and a Maxwell model and applied it to transient flows. De Kee and Chan<sup>11,45</sup> further combined the Liu model<sup>10</sup> with some well-known rheological models to study a complex mixture behavior including thixotropy and shear-thinning/(thickening). In Ref. 46, the De Kee–Chan Man Fong model was further investigated in large amplitude oscillatory shear flows for a filled polymer melt.

Almost all the reported models share a common feature in that there are two time scales: (i) a microstructure time scale in the kinetics equation and (ii) a relaxation time (macro-scale) of the continuum model. These models are very good in the prediction of viscoelasticity as well as thixotropy in different flows for multi-phase mixtures, for example, a mixture of colloidal solid particles in a viscoelastic matrix where the length/time scale in the suspending matrix and the length/time scale of the suspended structure are vastly different. In some cases, if viscoelasticity is mainly induced by the microstructure evolution (or single-phase), the same length/time scale should result and depends on the flow process.

In this work, we deal with a specific time dependence of the stress on the microstructure which is evolving in the flow

process—thus our model may be regarded as a microstructure-induced thixotropy and viscoelasticity model. Both the thixotropy and the relaxation of the viscoelasticity have a marginal difference in the length/time scale and can be modeled simultaneously from the microstructure approach (Lodge–Yamamoto network theory).<sup>42–44,47</sup> For the materials, we specifically think of a particulate suspension such as clay sediment, which has been widely studied in both numerical and experimental works.<sup>19,20,48</sup> The interaction of clay particles includes a short-range repulsive (Born) force and a long-range attractive (van der Waals) force.<sup>49</sup> Depending on interparticle distances, the resultant force can be either attraction or repulsion. When the two forces reach equilibrium, clay particles create a microstructure network that results in viscoelastic, shear-thinning, and thixotropic behavior. The particle interactions can be modeled by a network of springs,<sup>37</sup> which is similar to network strands of polymeric liquids.

The rest of this paper is structured in the following manner. The proposed constitutive model is described in Sec. II. Section III then gives a description of model predictions including stress overshoot, constant structure curves, viscosity bifurcation phenomenon, and the structure changing in amplitude oscillation flows for a typical thixotropic mixture (e.g., clay). Some concluding remarks are presented in Sec. IV.

### III. PROPOSED MODEL

In the proposed model, the relevant microstructure is a network of mechanical links used to model the interaction between any two junctions. Each link is confined between two temporary junctions and is represented by  $\mathbf{R}$  (Fig. 2); the probability distribution function (PDF)  $f(t, \mathbf{R})$  is interpreted in the sense that  $f(t, \mathbf{R})d^3\mathbf{R}$  represents the probability of finding a segment between  $\mathbf{R}$  and  $\mathbf{R} + d\mathbf{R}$  at time  $t$ . Here,  $f$  plays the role of the scalar structure parameter of structural kinetics theory; the description is probabilistic in nature as opposed to structural deterministic represented by Eq. (1); otherwise the model is the same. Note that  $f$  is non-negative and

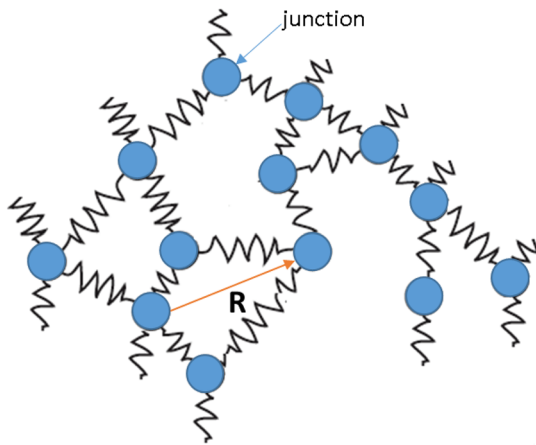


FIG. 2. A typical microstructure network and the  $\mathbf{R}$  vector.

vanishes at infinity. This type of description has been used in the works of Yamamoto,<sup>42</sup> Lodge,<sup>47</sup> Wiegel,<sup>50</sup> Wiegel and de Bats,<sup>51</sup> Phan-Thien and Tanner,<sup>52</sup> and Phan-Thien,<sup>53</sup> to name a few, in modeling polymeric liquids. The development of the theory follows that of Phan-Thien and Tanner, which is only briefly described here.

The simplest model for the build-up microstructure is

$$\frac{\partial}{\partial t}f(t, \mathbf{R}) + \dot{\mathbf{R}} \cdot \nabla f(t, \mathbf{R}) = g(\mathbf{R}) - \lambda_0^{-1}h(\dot{\gamma})f(t, \mathbf{R}), \quad (18)$$

where the rate of microstructure creation is  $g$ , an isotropic function of  $\mathbf{R}$ , and the rate of microstructure destruction is  $\lambda_0^{-1}h(\dot{\gamma})$ , where  $\lambda_0$  is a time constant and  $h(\dot{\gamma})$  is a (dimensionless) increasing function of the strain rate—in the limit of the zero strain rate  $h \rightarrow 1$ ; a simple form for this may be  $h(\dot{\gamma}) = (1 + \beta\dot{\gamma})$ , in which  $\beta$  is a parameter, and  $\dot{\gamma} = \sqrt{2\text{tr}\mathbf{D}^2}$  is the generalized strain rate, where  $\mathbf{D} = (\mathbf{L} + \mathbf{L}^T)/2$  is the strain rate tensor and  $\mathbf{L} = \nabla\mathbf{u}^T$  is the velocity gradient tensor ( $\mathbf{u}$  is the velocity) and the superscript  $T$  denotes a transpose operation. The possibility of a multimodal distribution for  $\mathbf{R}$ ,  $i = 1, \dots, N$  is envisaged, but not attempted here for simplicity. There are other formalisms of the model including those of Wiegel,<sup>50</sup> Wiegel and de Bats,<sup>51</sup> and Green and Tobolsky,<sup>54</sup> and the elegant approach detailed in the work of Bird *et al.*<sup>55</sup> We prefer this approach. All lead to the equations of balance.

The equilibrium distribution for  $f$  is

$$f_e = \lambda_0 h^{-1}(\dot{\gamma})g(\mathbf{R}). \quad (19)$$

Equation (18) is sometimes known as the Liouville equation. By multiplying Eq. (18) by any function  $Q$  of the segment vector  $\mathbf{R}$  and then integrating over all configuration space, the equation of change for  $Q$  can be derived<sup>55</sup> (assuming that  $f$  vanishes as fast as required at infinity),

$$\frac{d}{dt}\langle Q \rangle + \lambda_0^{-1}h(\dot{\gamma})\langle Q \rangle = \left\langle \dot{\mathbf{R}} \frac{\partial Q}{\partial \mathbf{R}} \right\rangle + [Q], \quad (20)$$

where  $[\cdot]$  denotes an average of “ $\cdot$ ” with respect to  $f$ .

We assume that the network junctions move in a non-affine manner, leading to

$$\dot{\mathbf{R}} = \mathbf{L}\mathbf{R} - \zeta\mathbf{D}\mathbf{R}, \quad (21)$$

where  $\zeta$  is a model parameter. This has worked well for polymer liquids and for suspensions of particles, where  $\zeta$  can be related to the particle aspect ratio.<sup>56,57</sup>

Then, from the equation of change (20),

$$\begin{aligned} \frac{d}{dt}\langle \mathbf{R}\mathbf{R} \rangle &= (\mathbf{L} - \zeta\mathbf{D})\langle \mathbf{R}\mathbf{R} \rangle + \langle \mathbf{R}\mathbf{R} \rangle(\mathbf{L} - \zeta\mathbf{D})^T \\ &+ \int [g - \lambda_0^{-1}h(\dot{\gamma})f]\mathbf{R}\mathbf{R}d^3\mathbf{R}, \\ &= (\mathbf{L} - \zeta\mathbf{D})\langle \mathbf{R}\mathbf{R} \rangle + \langle \mathbf{R}\mathbf{R} \rangle(\mathbf{L} - \zeta\mathbf{D})^T \\ &- \lambda_0^{-1}h(\dot{\gamma})\langle \mathbf{R}\mathbf{R} \rangle + \bar{g}\mathbf{I} \end{aligned}$$

or

$$\begin{aligned} \frac{d}{dt}\langle \mathbf{R}\mathbf{R} \rangle - (\mathbf{L} - \zeta\mathbf{D})\langle \mathbf{R}\mathbf{R} \rangle - \langle \mathbf{R}\mathbf{R} \rangle(\mathbf{L} - \zeta\mathbf{D})^T \\ + \lambda_0^{-1}h(\dot{\gamma})\langle \mathbf{R}\mathbf{R} \rangle = \bar{g}\mathbf{I}, \end{aligned} \quad (22)$$

where

$$\bar{g} = \frac{1}{3} \int g(\mathbf{R}) R^2 d^3\mathbf{R}. \quad (23)$$

This leads to

$$\begin{aligned} & \lambda \left\{ \frac{d}{dt} \langle \mathbf{RR} \rangle - (\mathbf{L} - \zeta \mathbf{D}) \langle \mathbf{RR} \rangle - \langle \mathbf{RR} \rangle (\mathbf{L} - \zeta \mathbf{D})^T \right\} + \langle \mathbf{RR} \rangle \\ & = \frac{R_0^2}{3h(\dot{\gamma})} \mathbf{I}, \end{aligned} \quad (24)$$

where

$$\lambda = \frac{\lambda_0}{h(\dot{\gamma})} \quad (25)$$

and

$$R_0^2 = 3\bar{g}\lambda_0 \quad (26)$$

is the no-flow mean square distance between a pair of junctions. Note that the break-up rate of the network is manifested in the relaxation time and the mean square distance—the higher the strain rate, the larger the  $h(\dot{\gamma})$ , and the lower the relaxation time (and hence elasticity) and the mean square distance between a pair of junctions.

Now, the stress contributed by the network, or the stress rule, is given by  $\tau^{(p)} = \langle H\mathbf{RR} \rangle$ , where  $H$  is the entropic spring stiffness for a network segment.<sup>42,47,52</sup> It is also valid for a suspension of ellipsoidal particles.<sup>58</sup> The constitutive equation for the stress is then given by

$$\begin{aligned} & \frac{\lambda_0}{h(\dot{\gamma})} \left\{ \frac{d}{dt} \tau^{(p)} - (\mathbf{L} - \zeta \mathbf{D}) \tau^{(p)} - \tau^{(p)} (\mathbf{L} - \zeta \mathbf{D})^T \right\} + \tau^{(p)} \\ & = \frac{HR_0^2}{3h(\dot{\gamma})} \mathbf{I}. \end{aligned} \quad (27)$$

Instead of working with  $\tau^{(p)}$ , we may define

$$\tau^{(p)} = \frac{HR_0^2}{3h(\dot{\gamma})} \mathbf{I} + \mathbf{S}^{(p)}, \quad (28)$$

where the extra stress  $\mathbf{S}^{(p)}$  is given by

$$\begin{aligned} & \frac{\lambda_0}{h(\dot{\gamma})} \left\{ \frac{d}{dt} \mathbf{S}^{(p)} - (\mathbf{L} - \zeta \mathbf{D}) \mathbf{S}^{(p)} - \mathbf{S}^{(p)} (\mathbf{L} - \zeta \mathbf{D})^T \right\} + \mathbf{S}^{(p)} \\ & = 2 \frac{\eta_{p0}}{h(\dot{\gamma})^2} \mathbf{D}, \end{aligned} \quad (29)$$

with

$$\eta_{p0} = \frac{HR_0^2\lambda_0(1-\zeta)}{3}, \quad \eta_p = \frac{\eta_{p0}}{h(\dot{\gamma})^2}, \quad \lambda = \frac{\lambda_0}{h(\dot{\gamma})}. \quad (30)$$

To this constitutive equation (29), we may add a Newtonian stress  $2\eta_s\mathbf{D}$ —as has been done in suspension mechanics. Thus, our microstructure-induced thixotropy model consists of

$$\mathbf{S} = 2\eta_s\mathbf{D} + \mathbf{S}^{(p)}, \quad (31)$$

where  $\eta_s$  is the solvent viscosity and  $\mathbf{S}^{(p)}$  is given by (29).

For a constant shear rate flow, the stress equations are

$$\begin{aligned} S_{11}^{(p)} + \lambda \frac{d}{dt} S_{11}^{(p)} - (2 - \zeta) \lambda \dot{\gamma} S_{12}^{(p)} &= 0, \\ S_{22}^{(p)} + \lambda \frac{d}{dt} S_{22}^{(p)} + \zeta \lambda \dot{\gamma} S_{12}^{(p)} &= 0, \\ S_{12}^{(p)} + \lambda \frac{d}{dt} S_{12}^{(p)} - \left(1 - \frac{\zeta}{2}\right) \lambda \dot{\gamma} S_{22}^{(p)} + \frac{\zeta}{2} \lambda \dot{\gamma} S_{11}^{(p)} &= \eta_p \dot{\gamma}. \end{aligned} \quad (32)$$

In small amplitude oscillatory shear flow with shear strain  $\gamma = \gamma_0 \sin \omega t$ ,  $\varepsilon \ll 1$ ,

$$\begin{aligned} \dot{\gamma} &= \omega \varepsilon \cos \omega t, \\ S_{12}^{(p)} &= \varepsilon (S_{12}^c \cos \omega t + S_{12}^s \sin \omega t) + HOT, \end{aligned}$$

$$\begin{aligned} S_{12}^c \cos \omega t + S_{12}^s \sin \omega t + \lambda \omega (-S_{12}^c \sin \omega t + S_{12}^s \cos \omega t) \\ = \eta_0 \omega \cos \omega t, \end{aligned}$$

$$S_{12}^c + \lambda \omega S_{12}^s = \eta_p \omega, \quad S_{12}^s - \lambda \omega S_{12}^c = 0,$$

$$S_{12}^s = \frac{\eta_0 \lambda \omega^2}{(1 + \lambda^2 \omega^2)}, \quad S_{12}^c = \frac{\eta_0 \omega}{(1 + \lambda^2 \omega^2)}.$$

The dynamic properties are given by

$$\eta' = \frac{\eta_0}{(1 + \lambda^2 \omega^2)}, \quad \eta'' = \frac{\eta_0 \lambda \omega}{(1 + \lambda^2 \omega^2)}. \quad (33)$$

It is noted that

- The proposed model involves the estimation of four empirical parameters. Three of them, i.e., the solvent viscosity  $\eta_s$ , the fully structured viscosity  $\eta_{p0}$ , and  $h(\dot{\gamma})$  function, are found through the equilibrium flow curve. The highest relaxation time  $\lambda_0$  can be obtained from an oscillatory experiment with frequency sweep.
- When  $\zeta = 0$ , one has a similar form of the simple thixotropic model (9), but the viscosity is inversely proportional to  $h(\dot{\gamma})^2$  instead of  $h(\dot{\gamma})$ ,

$$\frac{\lambda_0}{h(\dot{\gamma})} \frac{d}{dt} S_{12}^{(p)} + S_{12}^{(p)} = \frac{\eta_{p0}}{h(\dot{\gamma})^2} \dot{\gamma}. \quad (34)$$

- The isotropic assumption of  $g(\mathbf{R})$  may be a simplification in the network theory; however, if the creation rate is to depend on  $f$ , one can always separate out an isotropic term, and the rest can be assigned to the destruction rate.
- Recently, a new interpretation of yield stress was reported in Ref. 59. In this work, yielding is considered a kinetic process of a solid to fluid transition. Figure 3 shows the two regions in the relation between the relaxation time  $\lambda_0/h(\dot{\gamma})$  and the shear rate  $\dot{\gamma}$ . Below the yield point, at a large value of  $\lambda_0/h(\dot{\gamma})$ , the microstructure is fully structured, and the predicted stress of the model response resembles that of a Maxwell solid. As the microstructure network disintegrates to small flocs [ $\lambda_0/h(\dot{\gamma})$  is small], the interaction between different flocs would result in an elastic response (due to non-affine motion of the flocs) and a thixotropy viscosity (due to

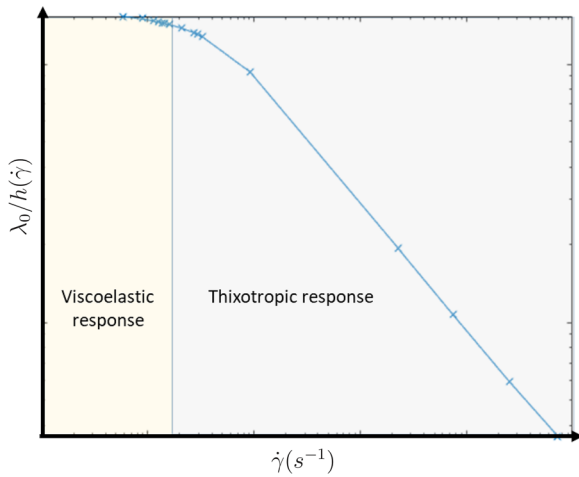


FIG. 3. The relaxation time vs the shear rate.

the integrated/disintegrated processes) as well. The model would be considered to be a thixotropic model, which is comparable to the model in Eq. (9), but the structure parameter is interpreted in a probabilistic sense (which has been integrated into the stress equations), rather than a scalar in simple thixotropic models.

#### IV. MODEL PREDICTIONS

##### A. Steady flow curve

At steady state,

$$S_{12}^{(p)} = \frac{\eta_p}{1 + \zeta(2 - \zeta)\lambda^2\dot{\gamma}^2} \dot{\gamma}, \tag{35}$$

$$S_{11}^{(p)} = (2 - \zeta)\lambda\dot{\gamma}S_{12}^{(p)}, \quad S_{22}^{(p)} = -\zeta\lambda\dot{\gamma}S_{12}^{(p)}. \tag{36}$$

This leads to the normal stress difference ratio

$$\frac{N_2}{N_1} = \frac{S_{22}^{(p)} - S_{33}^{(p)}}{S_{11}^{(p)} - S_{22}^{(p)}} = -\frac{\zeta}{2} \tag{37}$$

and the first normal stress difference

$$N_1 = 2\eta_{p0}\lambda_0\dot{\gamma}^2/h.$$

The shear stress is given by

$$S_{12} = \eta_s\dot{\gamma} + \frac{\eta_p\dot{\gamma}}{1 + \zeta(2 - \zeta)\lambda^2\dot{\gamma}^2}, \tag{38}$$

or the viscosity is

$$\begin{aligned} \eta &= \frac{S_{12}}{\dot{\gamma}} = \eta_s + \frac{\eta_p}{1 + \zeta(2 - \zeta)\lambda^2\dot{\gamma}^2} \\ &= \eta_s + \frac{\eta_{p0}}{(h^2 + \zeta(2 - \zeta)\lambda_{p0}^2\dot{\gamma}^2)}. \end{aligned} \tag{39}$$

Thus, if the fitting equation for the experiment viscosity data is  $\eta_{exp}$ , then

$$\frac{\eta_{p0}}{(h^2 + \zeta(2 - \zeta)\lambda_{p0}^2\dot{\gamma}^2)} = \eta_{exp} - \eta_s \tag{40}$$

$$h^2 = \frac{\eta_{p0}}{\eta_{exp} - \eta_s} - \zeta(2 - \zeta)\lambda_{p0}^2\dot{\gamma}^2.$$

$\eta_{exp}$  can be any convenient empirical curve used to fit the experimental data. These will provide a mean for choosing  $f_e$ , or  $h$ , over a range of the shear rate.

Thus, if Papanastasiou’s model<sup>60</sup> is chosen as the fitting equation for the experiment viscosity data, accounting for its engineering yielding behavior,

$$\eta(\dot{\gamma}) = \mu + \frac{S_y[1 - \exp(-n\dot{\gamma})]}{\dot{\gamma}}, \tag{41}$$

where  $\mu$  is the high shear viscosity,  $S_y$  is the yield stress value, and  $n$  is a parameter, then by choosing  $\mu = \eta_s$  and  $\eta_{p0} = nS_y$ , this provides a mean for determining  $h(\dot{\gamma})$ ,

$$h(\dot{\gamma}) = 1 + \beta\dot{\gamma}, \tag{42}$$

where  $\beta = \sqrt{\frac{n}{(1 - e^{-n})\dot{\gamma}} - \zeta(2 - \zeta)\lambda_0^2} - 1/\dot{\gamma}$ .

A range of applied shear rates is  $\dot{\gamma} = (4 \times 10^{-4} \rightarrow 10) \text{ s}^{-1}$ , with fine distribution at the low shear zone for a finer measurement of the fluid behavior. For each step of the applied shear rate, the system is sheared until reaching the equilibrium state. Figure 4 plots the equilibrium curve viscosity vs shear rate [Eq. (39)] and experimental data for the 3% bentonite mixture. It can be seen that the larger the value of  $n$ , the higher the low shear viscosity (the curve is thus more asymptotic to a Bingham fluid).

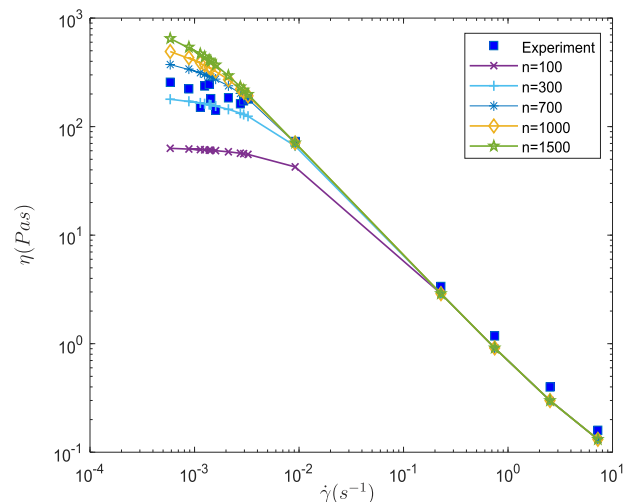


FIG. 4. A 3% bentonite mixture (blue square—experimental data) and viscosity flow curves [Eq. (39)] [a high shear viscosity of  $4.2 \times 10^{-2} \text{ Pa s}$ ,  $h$  calculated from Eq. (42), a yield stress of  $S_y = 0.65 \text{ Pa}$ , and growth parameter  $n = \{100, 300, 700, 1000, 1500\}$ ]. The fluid is allowed to attain the steady state at each shear step.

## B. Stress overshoot

Stress overshoot is an important phenomenon that happens when a thixotropic liquid undergoes a sudden change in applied strained rates (e.g., sediment flows over a fixed pipeline or blades moving in a mixer underwent a step change in the flow rate). Stress overshoot can be found in a step-change-in-shear rate experiment.<sup>25</sup> Each shear rate value of the equilibrium curve has a corresponding structural level. Then, with stepwise changes in the shear rate, the microstructure does not have sufficient time to adapt to the new equilibrium state. The inhomogeneous microstructure (hence viscosity) leads to stress overshoot that is linked to the flow process. A detailed explanation can be found in Ref. 6.

In this control shear rate mode, a step shear with a high  $\frac{d\dot{\gamma}}{dt}$  is applied. It is noted that the shear stress is now greater than  $S_y$ ; thus, the model is in a thixotropic response. The development of shear viscosity can be calculated from Eq. (32),

$$\frac{d}{dt}\eta^{(p)} + \lambda^{-1}\eta^{(p)} - \left(1 - \frac{\zeta}{2}\right)S_{22}^{(p)} + \frac{\zeta}{2}\dot{\gamma}S_{11}^{(p)} = \eta_{p0}(\lambda_0 h)^{-1}. \quad (43)$$

In the following, we demonstrate the use of the proposed constitutive model in a shear flow with a prescribed shear rate history. This was done by shearing a sample at a reference shear rate  $\dot{\gamma} = \dot{\gamma}_a$ . A higher step-change in speed  $\dot{\gamma} = \dot{\gamma}_b$  is then made, and the evolution of stress  $S_b$  is noted before  $\dot{\gamma}$  is reversed into  $\dot{\gamma}_b$ . Three scenarios of shear rate histories are carried out. A shear rate  $\dot{\gamma}$  of  $4 \text{ s}^{-1}$  is maintained until equilibrium state is attained, subsequently increased from  $4 \text{ s}^{-1}$  to  $7 \text{ s}^{-1}$  in 1 s for case (a) [and 4 s and 6 s for case (b) and (c), respectively], continued at  $7 \text{ s}^{-1}$  in 10 s, reduced from  $7 \text{ s}^{-1}$  to  $4 \text{ s}^{-1}$  in 1 s, and kept at  $4 \text{ s}^{-1}$  for the rest. The actual variation in the imposed shear rate can be fitted by the following exponential functions, as illustrated in the lower parts of Fig. 6:

$$\begin{aligned} \dot{\gamma}_{4-7} &= 4e^{-6(t-t_0)} + 7[1 - e^{-6(t-t_0)}], \\ \dot{\gamma}_{7-4} &= 7e^{1.5\frac{(t-t_0)}{(t_0-0.5)}} + 4\left[1 - e^{1.5\frac{(t-t_0)}{(t_0-0.5)}}\right]. \end{aligned}$$

The microstructure-induced thixotropy is now examined numerically by an ordinary differential equation (ODE) solver. Here, we choose the ODE23s solver in Matlab due to the stiffness of the problem. To simulate the time-dependent rheological behavior, the rheological equation (43) is employed. The value of  $\lambda_0$  is to be calculated as  $1/(2\pi f_0)$  at the intersection point between the storage modulus ( $G'$ ) and the dissipative modulus ( $G''$ ) in frequency sweep experiments (Fig. 5). Here, the maximum value of the relaxation time  $\lambda_0$  is estimated around 40 s; the value of  $h(\dot{\gamma})$  of each steady shear rate is calculated from Eq. (42). The numerical simulation shows the development of shear stress with the applied shear rate (when  $\dot{\gamma}$  from  $4 \text{ s}^{-1}$  to  $7 \text{ s}^{-1}$ ). The top of Fig. 6 (Multimedia view) shows that the model has the ability to predict the general responses in all cases, including the maximum location of the stress at the transition of strain rate. As expected, a higher shear rate slope ( $\frac{d\dot{\gamma}}{dt}$ ) leads to a reduction of the stress overshoot peaks. Note that the break-up rate of the network is manifested in the relaxation time—the higher the strain rate, the larger the  $h(\dot{\gamma})$ , and the lower the relaxation time (and hence stress overshoot).

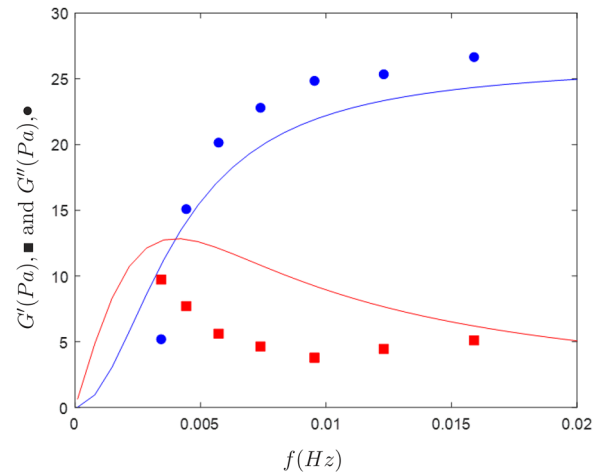


FIG. 5. Oscillatory frequency sweep experiment of the 3% bentonite clay. Continuous lines are  $G'$  (blue) and  $G''$  (red) approximated by multiplying  $\eta'$  and  $\eta''$  [Eq. (33)] by  $\omega$ .

## C. Constant structure curves

As reported in Ref. 25, a step-change shear rate experiment (Fig. 7) is carried out to evaluate the CS curves. It is recalled that a constant shear rate has a structural level relating to a CS curve; therefore, the experiment is performed by adopting one reference shear rate and then applying a higher or lower shear rate magnitude around this reference value. A 3% bentonite solution undergoes a reference shear rate  $\dot{\gamma} = \dot{\gamma}_r$  until the steady state is attained. Then, an increasing/decreasing shear rate  $\dot{\gamma} = \dot{\gamma}_i$  is imposed, and the highest/lowest value of shear stress  $S_1$  is recorded before  $\dot{\gamma}$  is reduced/increased to  $\dot{\gamma}_r$ . In this work, those repeated steps are carried out with  $\dot{\gamma}_r = \{2, 5, 8\} \text{ s}^{-1}$  and then graphed the family of CS curves. Following the same procedure of the Toorman model [Eqs. (11)–(16)], an equation of a constant structure curve is

$$S_{12} = (1 + h_1^{-2} - h^{-2})\eta_p\dot{\gamma} + \eta_s\dot{\gamma}. \quad (44)$$

The parameters  $\eta_s$  and  $\eta_p$  and the function  $h(\dot{\gamma})$  have been found from the Papanastasiou equilibrium flow curve with a viscosity of  $0.042 \text{ Pa s}$  and a yield stress of  $0.65 \text{ Pa}$  (which corresponds to a 3% bentonite solution having an equilibrium flow curve plotted in Fig. 4). A substitution of those values [ $\eta_s$ ,  $\eta_{p0}$ , and  $h(\dot{\gamma})$ ] of each CS curve in Eq. (44) gives a set of CS curves. As shown in Fig. 8, a comparison of the experimental data and CS curves calculated from the proposed model is plotted. It can be seen that the lower value of  $\dot{\gamma}_r$ , the higher yield stress is. A qualitative agreement between the model predictions and the experimental observations is observed.

## D. Viscosity bifurcation

Rheometric tests (Ref. 61) have revealed that for small stresses (lower than a given critical value), fluid viscosity rises over time



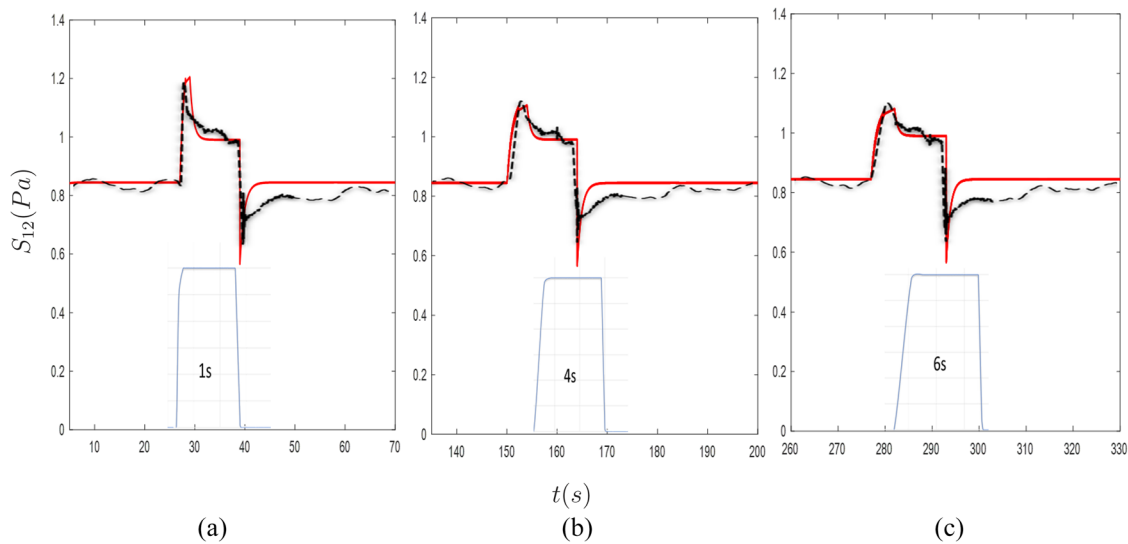


**FIG. 6.** Numerical calculation and experimental results for the stress response of a 3% wt bentonite clay mixture: [(a)–(c)] the corresponding shear stresses (red solid curve—experimental data, black dashed curve—model prediction) for the declining slope of shear rate over time; the smaller figures: time evolution of the applied shear rate. Multimedia view: <https://doi.org/10.1063/5.0033199.1>

and eventually prevents the fluid from flowing. On the other hand, larger stresses (above the critical stress value) result in a drop in viscosity continually over time and the fluid thus accelerates. Consequently, the viscosity changes in a discontinuous manner from a low value to an unbound value at the yield stress and this behavior is named viscosity bifurcation. Experiments were conducted<sup>61</sup> to study the bifurcation in rheological behavior of various materials.

We shall consider a  $j$  CS curve that intersects the EF curve at the equilibrium point J (Fig. 1). For points below the equilibrium flow curve, such as point 1, if the imposed shear stress  $S_1$  is maintained constant ( $S_1$  is smaller than the yield value), the structure will continuously develop and the shear viscosity  $\eta_1$  would increase until the fluid reaches the state of equilibrium ( $\eta_1 = \eta_{p0}$ , an extremely high value). On the other hand, at points above the

EF curve (e.g., point 2), if one keeps  $S_2$  (which is higher than the yield stress value), the microstructure will gradually collapse, resulting in a loss in the shear viscosity  $\eta_2$  and, eventually, to the equilibrium value  $\eta_\infty$ . If Papanastasiou’s model<sup>60</sup> is the fitting equation, shear viscosity is thus bounded by  $nS_y$  and  $\eta_\infty$ , hence the bifurcation.

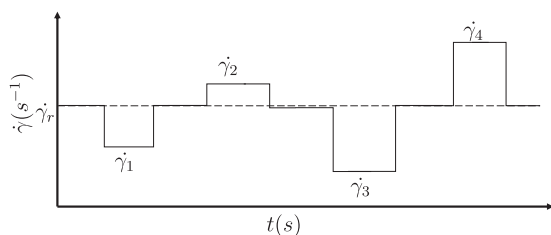


**FIG. 7.** A typical step-change shear rate experiment to graph the set of constant structure curves. A reference shear rate ( $\dot{\gamma}_r$ ) is chosen and then higher ( $\dot{\gamma}_2, \dot{\gamma}_4$ ) or lower shear rate ( $\dot{\gamma}_1, \dot{\gamma}_3$ ) magnitudes around this reference value are applied. It is noted that  $\dot{\gamma}_r$  has a structural level relating to a CS curve.

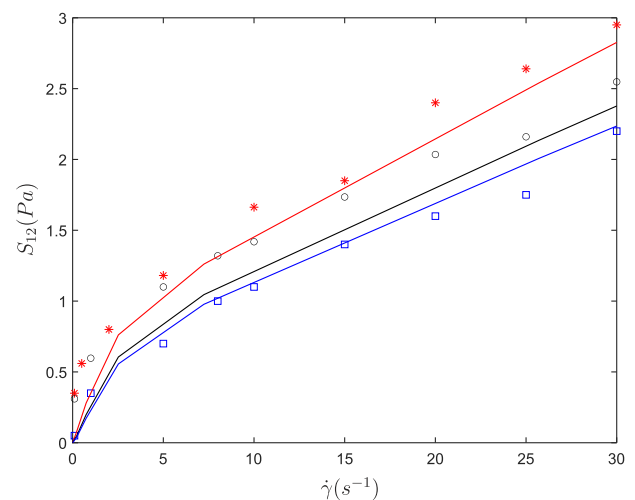


**FIG. 8.** A family of CSCs. Symbols: plotted from experimental data for reference shear rates  $\dot{\gamma}_r = 2 \text{ s}^{-1}$  (red line and red asterisk),  $5 \text{ s}^{-1}$  (black line and black open circle), and  $8 \text{ s}^{-1}$  (blue line and blue open square) (from top to bottom); solid line: calculated from the proposed model.

The model is then applied to predict the viscosity evolution of a bentonite suspension over time under a range of applied stresses. To carry out the test, the test samples are pre-sheared so that a reproducible initial state can be obtained. From the previous steady experiment conducted to analyze the yield stress, it was found that the yield stress for a 5 wt. % bentonite suspension is approximately around 10 Pa. Hence, applied stresses of {8, 9, 10, 11, 12} Pa are employed here to analyze the viscosity bifurcation [Fig. 9 (top)]. As anticipated, when the shear stress imposed to the sample is below the yield point, the structure builds-up, resulting in a more viscous dominant behavior. Viscosity thus asymptotes to a very large value. Nevertheless, when the shear stress applied exceeds the yield stress, the microstructure fails and the bentonite suspension viscosity is thus approximate to 0.05 Pa s. Figure 9 (bottom) shows the model

prediction of viscosity vs time using the same values of applied stresses.

### E. Oscillatory flows

This experiment involves imposing an increase in the amplitude oscillation stress at a fixed frequency and tracks the corresponding changes in the storage modulus ( $G'$ ) representing elastic components and the loss modulus ( $G''$ ) exhibiting viscous components of the fluid. The dominant modulus decides whether the mixture, under the applied stress, is to be regarded as an elastic or a viscous material. The stress amplitude is continually increased until  $G'$  and  $G''$  changed significantly with a stress threshold. Below this stress level, the microstructure network can resist the applied stress without a significant deformation. The mixture is able to store energy and recover its initial configuration (to some extent). It behaves like an elastic solid (not ideal), and some energy is dissipated. Thus, one has an elastic response ( $G' > G''$ ). Conversely, if the stress amplitude is sufficiently large, the structured network disintegrates and the energy exerted on the material is dissipated. Consequently, the material responds in a viscous manner ( $G' < G''$ ).

The oscillatory flow experiments are conducted on a bentonite suspension of 4 wt. %. The model's parameters are estimated from EFC curve (a viscosity of  $9.5 \times 10^{-2}$  Pa s, a yield stress of  $S_y = 7.68$  Pa), and  $h(\dot{\gamma})$  is calculated from Eq. (42) and the frequency sweep experiments ( $\lambda_0 = 3.18$  s). From the oscillatory sweep, due to the collapse of the microstructure, there is another way of interpreting the yield stress. One can consider the sudden drop of storage modulus  $G'$  to be the yield point, as this represents the breakdown of the structure, whereas others consider the crossover between  $G'$  and  $G''$  to be a critical point (yield) as it is the conversion from elastic to viscous behavior. As shown in Fig. 10,  $G'$  is approximately one order of magnitude larger than  $G''$  at a low-stress range, showing that the suspension is stable and shows

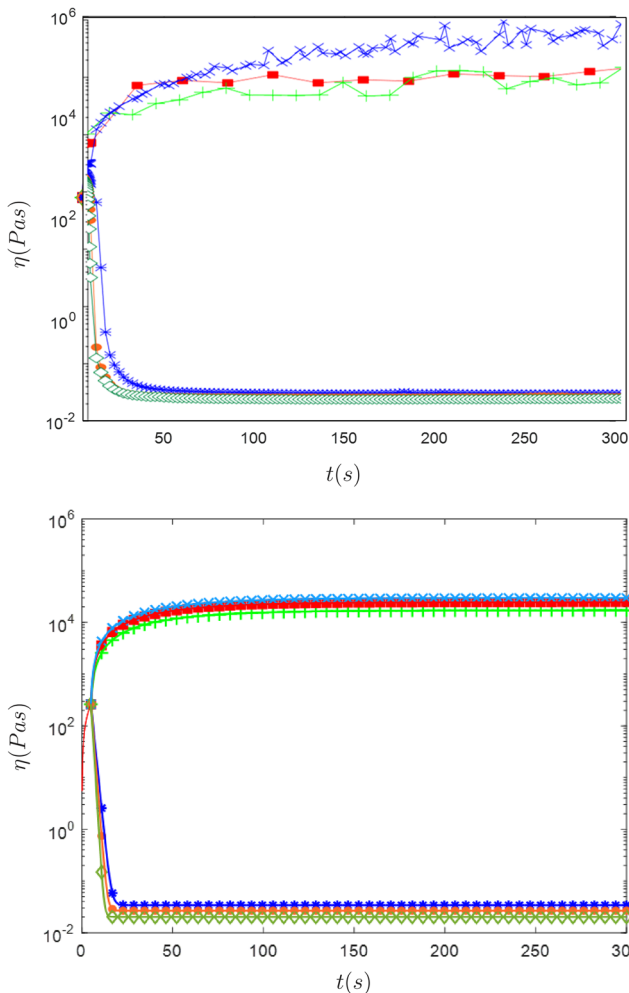


**FIG. 9.** (Top) Viscosity bifurcation for 5 wt. % bentonite suspensions. (Bottom) As predicted by the model for different applied stresses [8 (blue cross), 9 (red rectangle), 10 (green plus), 11 (blue asterisk), 12 (green closed diamond), and 13 (orange closed circle)] Pa.

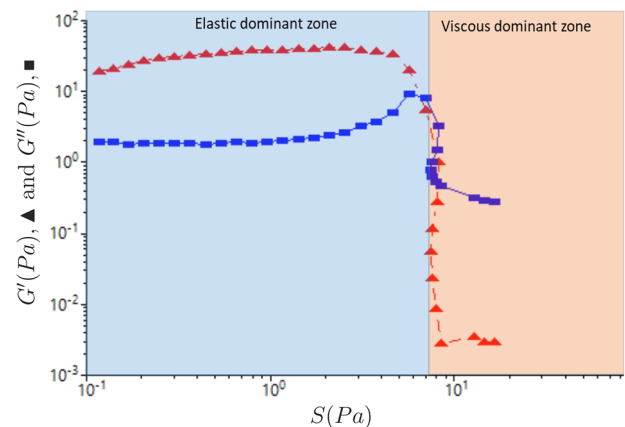


**FIG. 10.** Oscillatory stress sweep experiment at a fixed frequency (1 Hz) of the 4% bentonite clay. Viscoelastic response occurs at an applied stress below 7.68 Pa.

a gel-like response. When the stress amplitude gradually develops, a yield stress value can be determined around 7.68 Pa, which is also consistent with value deduced from the equilibrium flow curve.

Significant differences in the response of the mixture in oscillating flows can be shown by the Lissajous graphs. These Lissajous graphs are plots of stress vs strain, with each curve corresponding to an oscillatory shear test with a sinusoidal stress input at a fixed frequency and amplitude. In this test, we repeat this procedure for applied stresses of {2, 3.7, 4.7, 5.7, 7, 8, 10, 12} Pa at a fixed frequency

$f = 1$  Hz and then plot the set of curves, as shown in Figs. 11 and 12. The current theoretical analysis shows a good agreement with the experimental results in the phase transition changing from a solid to a liquid. The trajectory is an asymptote straight line for an elastic solid at small stresses [Figs. 11(a) and 11(b)]. With larger stresses, the trajectory becomes more elliptic in a viscoelastic zone [Figs. 11(c), 11(d), 12(a), and 12(b)]. At large enough stresses, the ellipse reduces to a circle, indicating that all network structures are practically broken and the material now resembles a Newtonian fluid [Figs. 12(c) and 12(d)].

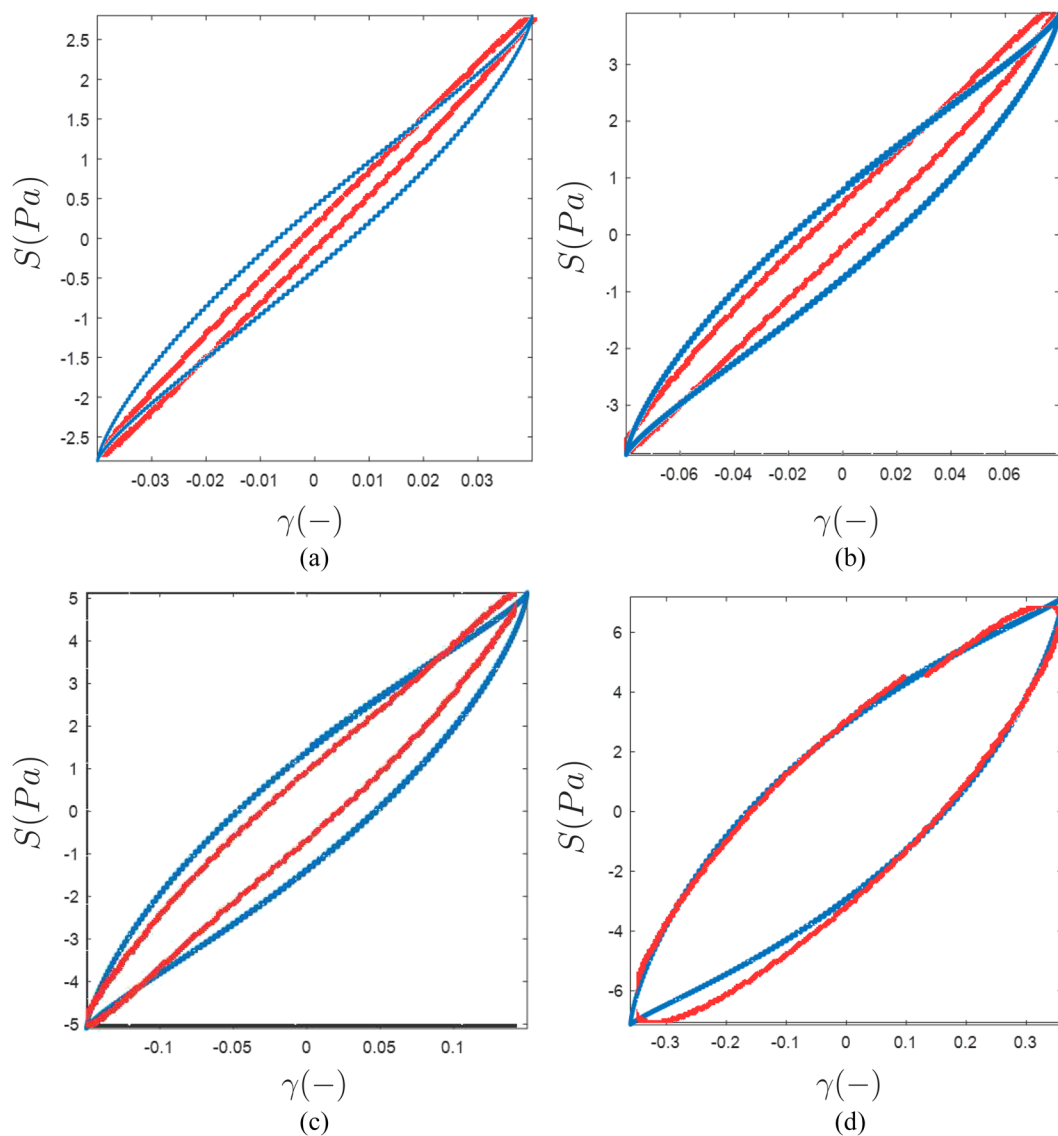


**FIG. 11.** Lissajous figures of oscillatory flow experiments and the model prediction on the 4% bentonite clay with increasing applied stresses of 2 Pa (a), 3.7 Pa (b), 4.7 Pa (c), and 5.7 Pa (d) at a frequency  $f = 1$  Hz. Red: data, blue: model.

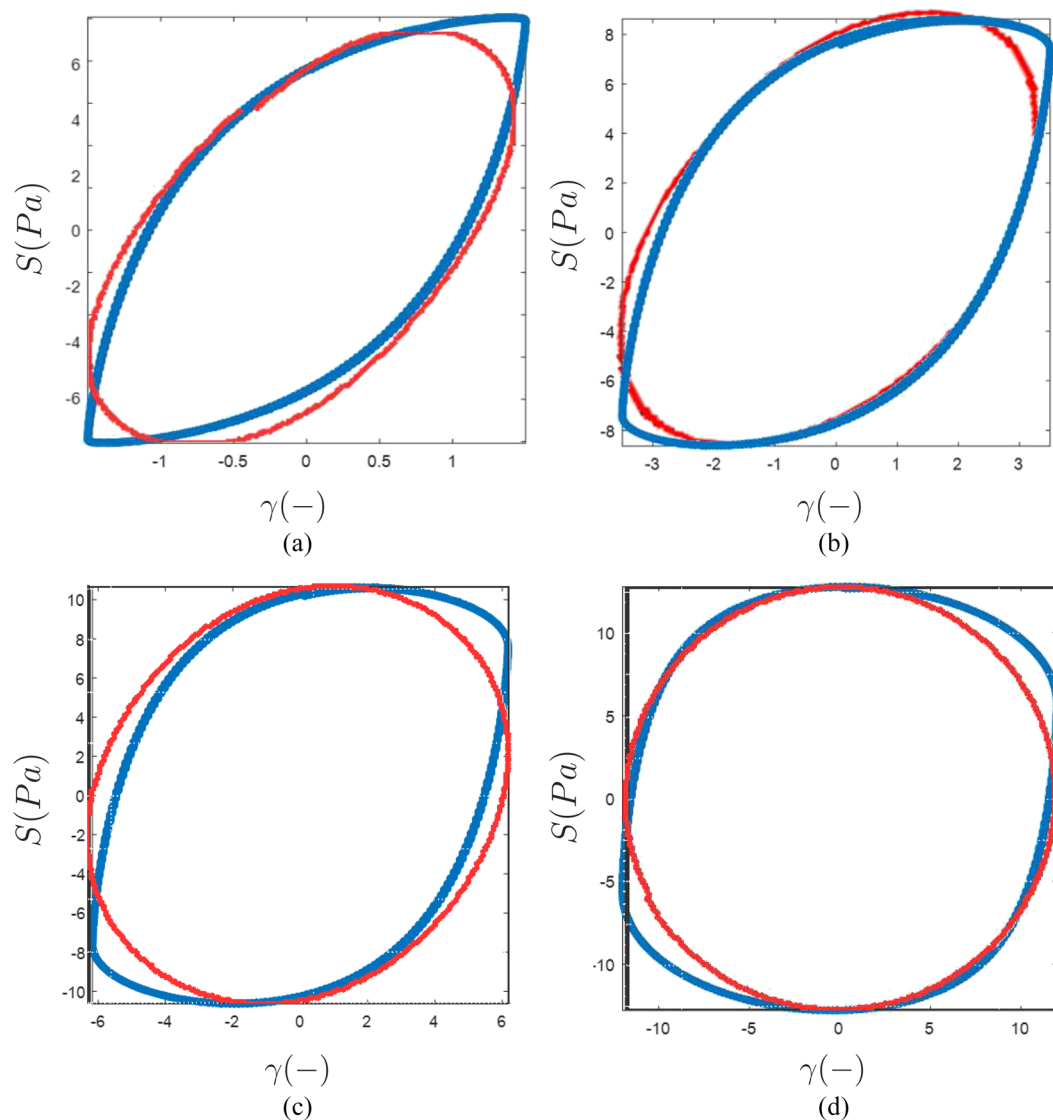


**FIG. 12.** Lissajous figures of oscillatory flow experiments and the model prediction on the 4% bentonite clay with increasing stress amplitude of 7 Pa (a), 8 Pa (b), 10 Pa (c), and 12 Pa (d) at a frequency  $f = 1$  Hz. Red: data, blue: model.

## V. CONCLUDING REMARKS

In this article, a simple model based on the network theory for viscoelastic–thixotropic mixtures is developed, and its predictions in a variety of shear and oscillatory shear flows are given. To model thixotropy–viscoelastic behaviors and assuming that both viscoelasticity and thixotropy are induced by microstructure networks, the proposed constitutive equation is fully specified from the microstructure configuration; no continuum viscoelastic model for the stress is required, and thus, the model has a small number of parameters and is convenient for engineering simulation tasks.

In contrast to the deterministic models proposed in the literature, the structural parameter here is a probability distribution function  $f(t, \mathbf{R})$ . The creation function  $g$  is isotropic, and the destruction function  $h$  is chosen by fitting experimental data with a shear-thinning (engineering yield stress) model. Its final form resembles the simple thixotropic model (9), but the relaxation time  $\lambda$  is inversely proportional to  $h$ , and the network contributed viscosity is inversely proportional to  $h^2$ .

From an engineering perspective, we believe that it is reasonable and practical to model a viscoelastic–thixotropy material as a fluid (at all stress levels) that has elasticity and extremely high viscosity at small shear rates (the concept of engineering yield stress),



- <sup>40</sup>M. M. Cross, “Rheology of non-Newtonian fluids: A new flow equation for pseudoplastic systems,” *J. Colloid Sci.* **20**, 417–437 (1965).
- <sup>41</sup>P. Doremus and J. M. Piau, “Yield stress fluid. Structural model and transient shear flow behaviour,” *J. Non-Newtonian Fluid Mech.* **39**, 335–352 (1991).
- <sup>42</sup>M. Yamamoto, “The visco-elastic properties of network structure I. General formalism,” *J. Phys. Soc. Jpn.* **11**, 413 (1956).
- <sup>43</sup>M. Yamamoto, “The visco-elastic properties of network structure III. Normal stress effect (Weissenberg effect),” *J. Phys. Soc. Jpn.* **13**, 1200 (1958).
- <sup>44</sup>M. Yamamoto, “The visco-elastic properties of network structure II. Structural viscosity,” *J. Phys. Soc. Jpn.* **12**(10), 1148–1158 (1957).
- <sup>45</sup>D. De Kee and C. F. Chan Man Fong, “Modelling of complex suspensions,” in *Theoretical and Applied Rheology*, edited by P. Moldenaers and S. Keunings (Elsevier Science Publishers, Oxford, Amsterdam, 1992), pp. 598–600.
- <sup>46</sup>R. S. Jeyaseelan and A. J. Giacomin, “Structural network theory for a filled polymer melt in large amplitude oscillatory shear,” *Polym. Gels Networks* **3**, 117–133 (1995).
- <sup>47</sup>A. Lodge, “The isotropy of Gaussian molecular networks and the stress-birefringence relations for rubber-like materials cross-linked in stressed states,” *Kolloid-Z.* **171**, 46 (1960); “Constitutive equations from molecular network theories for polymer solutions,” *Rheol. Acta* **7**, 379 (1968).
- <sup>48</sup>E. Bertevas, T. Tran-Duc, K. Le-Cao, B. C. Khoo, and N. Phan-Thien, “A smoothed particle hydrodynamics (SPH) formulation of a two-phase mixture model and its application to turbulent sediment transport,” *Phys. Fluids* **31**, 103303 (2019).
- <sup>49</sup>P. Coussot, *Mud Flow Rheology and Dynamics*, *IAHR Monographs* (Taylor & Francis, 1997).
- <sup>50</sup>F. W. Wiegel, “A network model for viscoelastic fluids,” *Physica* **42**, 156 (1969).
- <sup>51</sup>F. M. Wiegel and F. T. de Bats, “Rheological properties of a network model for macromolecular fluids,” *Physica* **43**, 33 (1969).
- <sup>52</sup>N. Phan-Thien and R. I. Tanner, “A new constitutive equation derived from network theory,” *J. Non-Newtonian Fluid Mech.* **2**, 353 (1977).
- <sup>53</sup>N. Phan-Thien, “A nonlinear network viscoelastic model,” *J. Rheol.* **22**, 259 (1978).
- <sup>54</sup>M. S. Green and A. V. Tobolsky, “A new approach to the theory of relaxing polymeric media,” *J. Chem. Phys.* **14**, 80 (1946).
- <sup>55</sup>R. B. Bird, C. F. Curtiss, R. C. Armstrong, and O. Hassager, *Dynamics of Polymeric Liquids*, Kinetic Theory, 2nd ed. (John Wiley & Sons, New York, 1987), Vol. 2.
- <sup>56</sup>Z. Ouyang, E. Bertevas, L. Parc, B. C. Khoo, N. Phan-Thien, J. Ferec, and G. Ausias, “A smoothed particle hydrodynamics simulation of fiber-filled composites in a non-isothermal three-dimensional printing process featured,” *Phys. Fluids* **31**, 123102 (2019).
- <sup>57</sup>J. Férec, E. Bertevas, B. C. Khoo, G. Ausias, and N. Phan-Thien, “A rheological constitutive model for semiconcentrated rod suspensions in Bingham fluids,” *Phys. Fluids* **29**, 073103 (2017).
- <sup>58</sup>N. Phan-Thien, in *Rheology of Non-Spherical Particle Suspensions*, edited by F. Chinesta and G. Ausias (Wiley-ISTE, London, 2015), pp. 2–17.
- <sup>59</sup>A. Malkin, V. Kulichikhin, and S. Ilyin, “A modern look on yield stress fluids,” *Rheol. Acta* **56**, 177–188 (2017).
- <sup>60</sup>T. C. Papanastasiou, “Flows of materials with yield,” *J. Rheol.* **31**(5), 385–404 (1987).
- <sup>61</sup>P. Coussot, Q. D. Nguyen, H. T. Huynh, and D. Bonn, “Viscosity bifurcation in thixotropic, yielding fluids,” *J. Rheol.* **46**(3), 573–589 (2002).
- <sup>62</sup>P. R. de Souza Mendes and R. L. Thompson, “A critical overview of elasto-viscoplastic thixotropic modeling,” *J. Non-Newtonian Fluid Mech.* **187–188**, 8–15 (2012).